Batteries & Supercaps

Research Article
doi.org/10.1002/batt.202400597

Chemistry Europe
European Chemical Societies Publishing

www.batteries-supercaps.org

Designer Fluorescent Redoxmer Self-Reports Side Reactions in Nonaqueous Redox Flow Batteries

Lily A. Robertson,*[a, b] Ilya A. Shkrob,*[a, b] Zhiguang Li,[a, b, d] Garvit Agarwal,[a, c, e] Zhou Yu,[a, c, f] Rajeev S. Assary,[a, c] Lei Cheng,[a, c, g] Lu Zhang,[a, b] and Zhengcheng Zhang[a, b]

The state of health (SOH) is a critical measure for evaluating and predicting performance of redox flow batteries (RFBs). However, diagnosing SOH of RFBs is often challenging due to the overwhelming complexity of the electrolytes and associated electrochemical reactions. Designing active molecules or redoxmers that can autonomously exhibit property changes upon specific stimuli may provide a viable way for early diagnosis of SOH. Herein, a dimerized redoxmer, **DGL-N-CH$_3$**, was designed and synthesized by linking blue-green fluorescent monomers through a diglycolamide linker. While **DGL-N-CH$_3$** still maintains similar electrochemical behavior and strong fluorescence, we observe a unique side reaction when cycling **DGL-N-CH$_3$** in H-cells, which leads to a side product, **NHCH$_3$-BzNSN** via linker cleavage. Interestingly, **NHCH$_3$-BzNSN** also emits fluorescence but at a longer wavelength. By taking advantage of this unique fluorescent change that corresponds to the growth of **NHCH$_3$-BzNSN**, we successfully established the capacity decay of **DGL-N-CH$_3$** H-cell cycling, exemplifying a proof-of-concept self-reporting redoxmer design towards *in situ* SOH monitoring.

1. Introduction

With the increasing adoption of renewable energy resources, such as wind and solar, integrating energy storage into grid becomes crucial to enable the time domain to ease the intermittent nature of those resources.[1] Redox flow batteries (RFBs) have been recognized as a promising candidate for large-scale energy storage solutions due to decoupled energy and power, low cost, and scalability. While several implementations of aqueous RFBs have been demonstrated at commercial relevant scales,[2] nonaqueous RFBs (NRFBs) provide an attractive option with wider electrochemical windows, more choices of redox materials, higher energy density, and possible lower cost. The introduction of organic redox-active molecules (redoxmers) in NRFBs brings significant advantages as these redoxmers are mostly made from cheap earth-abundant elements and can be readily engineered toward certain properties or functions, such as redox potential, solubility, stability, and even self-reporting.

Self-reporting is an emerging design function for redoxmers that could enable early diagnostics of undesired processes without interfering with RFB operations. Realizing such functions in a flow cell often requires an orthogonal property sensed by certain spectroscopy instruments that would not interfere with the electrochemical cycling operations. Some examples in the literature include *in situ* X-ray techniques,[3] advanced electrochemical characterization,[4] and, most frequently, UV-vis absorption monitoring.[5] The latter has been demonstrated for sensitive diagnostics[5b] capable of detecting specific degradation products.[5e] Optical methods are ideal for monitoring real-world RFB systems as they may be incorporated *in situ*, even at high concentrations, such as via fluidics or optical fiber.[6] Recent work by Zhao et al. examined degradation in aqueous anthraquinone RFBs using *in situ* NMR[7] and electron spin resonance monitoring.[8] Schuburt and co-workers demonstrated online monitoring in an aqueous nitroxide RFB by *in situ* infrared spectroscopy.[9] Fewer *in situ* studies have been published for nonaqueous systems but include infrared[10] and UV-vis[11] spectroscopy. In our previous study, we introduced fluorescence (FL) into a 2,1,3-benzothiadiazole (BzNSN) redoxmer via an acetamide group. This molecule is a liquid and miscible with the electrolyte, a common strategy for improving the redoxmer solubility and overall energy density of NRFBs.[12] By monitoring the non-invasive FL, we were able to track the

[a] *L. A. Robertson, I. A. Shkrob, Z. Li, G. Agarwal, Z. Yu, R. S. Assary, L. Cheng, L. Zhang, Z. Zhang*
Joint Center for Energy Storage Research

[b] *L. A. Robertson, I. A. Shkrob, Z. Li, L. Zhang, Z. Zhang*
Chemical Sciences and Engineering Division, Argonne National Laboratory, Lemont, IL 60439, USA
E-mail: robertla@anl.gov
shkrob@anl.gov

[c] *G. Agarwal, Z. Yu, R. S. Assary, L. Cheng*
Materials Science Division, Argonne National Laboratory, Lemont, IL 60439, USA

[d] *Z. Li*
Zhejiang ERG Energy Ltd. Co., Zhejiang Province, 317100, China

[e] *G. Agarwal*
Schrödinger, Inc., New York, NY 10036, USA

[f] *Z. Yu*
Department of Mechanical Engineering, University of Alabama, Tuscaloosa, AL 35487, USA

[g] *L. Cheng*
Chemical Sciences Division, Oak Ridge National Laboratory, Oak Ridge, TN 37830, USA

Supporting information for this article is available on the WWW under https://doi.org/10.1002/batt.202400597

Research Article
doi.org/10.1002/batt.202400597
Chemistry Europe
European Chemical Societies Publishing

redoxmers in H-cells in real time that revealed the *in situ* crossover behavior of the acetamide BzNSN through selected membranes.[13] While the demonstration was successful, more effort is needed to expand the possible use scenarios and implement more sophisticated detection schemes, such as *in situ* monitoring state of health (SOH) of NRFBs. Importantly, validation of properties such as solubility, cycling and calendar stability, and redox potential are needed for any redoxmer and can be optimized by molecular engineering.[14] Operando methods are an added tool to correlate spectroscopic signatures with battery performance.

Here, we report a designer redoxmer dimer extended from our previous monomer design. While this dimer resembles the monomer in terms of electrochemical performance and strong FL emission, the unique evolution of the FL over the course of H-cell cycling reflects the changes of the redoxmer and leads to discovery of the decomposition pathway, representing a very promising approach to monitor the SOH of RFBs.

2. Results and Discussion

The dimer redoxmer design combines the BzNSN units through a diglycolamide linker, which also enabled the FL emission. Briefly, we acylated 4-amino-2,1,3-benzothiadiazole with diglycoyl chloride to give the secondary amide dimer, **DGL-N-H**, which was subsequently alkylated using cesium carbonate as a base to give the tertiary amide dimer, **DGL-N-CH$_3$** (Scheme 1, full synthetic details in Section S1). Before proceeding further, we briefly consider structural underpinnings of this design strategy.

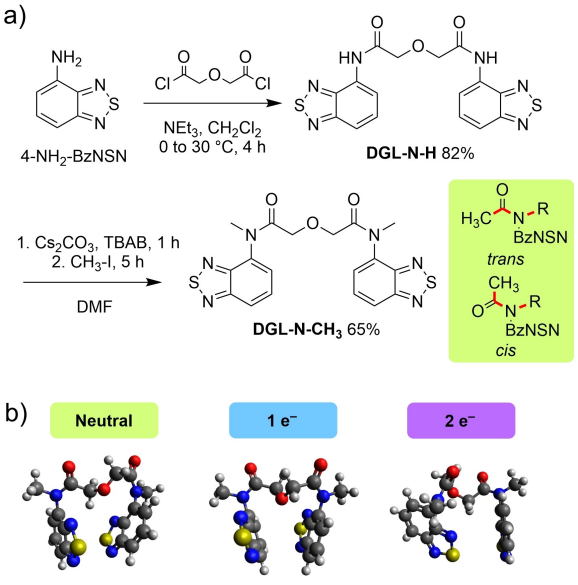

Scheme 1. a) Stepwise synthesis of the BzNSN dimer **DGL-N-CH$_3$** (drawn as the *trans-trans* isomer); b) optimized geometries vs. oxidation state for the *trans-trans* (*tt*) isomer of **DGL-NCH$_3$**.

2.1. Stereochemistry

The amide stereochemistry is interesting. Amide bonds have partial ionic character, so the C–N bond rotation is frustrated; thus, in **DGL-N-CH$_3$** (Scheme 1), the two BzNSN pendants can be either in *cis*- (*c*) or *trans*- (*t*) position relative to the carbonyl oxygens in the amide groups. Like all dimeric amides, the dimer shown in Scheme 1could exist in the *cc*, *ct*, and *tt* conformations (*ct* and *tc* are equivalent due to symmetry). The ^{1}H NMR spectra of **DGL-N-CH$_3$** shows no isomerism at 25 °C, i.e., the molecule is "locked" in a single conformation. In the polarized continuum DFT model (see Section S2 and Table S1), the *tt* isomer of **DGL-N-CH$_3$** has the lowest energy with $tt < ct \ll cc$. This ordering remains when the molecule is singly (^{2}AA$^{\bullet-}$) or doubly charged (^{3}A$^{\bullet-}$A$^{\bullet-}$) with the triplet diradical also being the most stable electronic state. Thus, we assume that the dimer molecule is permanently locked in the *tt* conformation in all states of charge. According to our molecular dynamics calculations (Section S2 and Figure S1), in this *tt* conformation, the minimal separation between the two BzNSN groups is >6 Å in all states of charge, so intramolecular interaction is weak. Via these simulations, we also evaluated clustering and dynamics with varied supporting electrolytes; however, tetrabutylammonium hexafluorophosphate (NBu_4PF_6) was chosen for the primary experiments as it exhibited the best stability with the DGL series.

2.2. Cyclic Voltammetry

The design of **DGL-N-CH$_3$** ensures a similar stable electrochemical behavior as compared to our previously reported "monomer" **CH$_3$-AcBzC$_6$** containing only one BzNSN unit attached with an acetamide group.[13] The **DGL-N-CH$_3$** dimer has reversible cyclic voltammetry (CV), both in scan rate analysis (Figure 1a) and repeated scanning (Section S3 and Figure S2a), with a half-wave potential ($E_{1/2}$) of −1.64 V vs. Ag/Ag$^+$ in 0.5 M NBu_4PF_6/CH_3CN, close to the predicted value of −1.66 V vs. Ag/Ag$^+$ and very similar to the $E_{1/2}$ of **CH$_3$-AcBzC$_6$** (Figure 1b, −1.67 V vs. Ag/Ag$^+$). The ratios of the extrapolated anodic and cathodic peak currents, i_{ap}/i_{ac}, were close to unity, showing reversibility on the CV time scale (see Table S2). The diffusion coefficients calculated from the scan rate analysis are 2.7 and 18×10^{-5} cm^2/s, respectively, for the dimer and monomer (see Table S3 and Figure S2d).

Oligomeric designs are a common molecular engineering strategy for reducing redoxmer crossover in NRFBs.[15] Our dimeric design is aimed at understanding the performance of BzNSN-derived multimers. The first stark effect was very low solubility of **DGL-N-CH$_3$** (~10 mM in 0.5 M NBu_4PF_6 in CH_3CN) compared to the miscible liquid monomer. Two additional dimeric derivatives were synthesized with ethyl (**Et**) and ethylene glycol (**EG**) groups. The former barely improved solubility while the latter improved to ~150 mM in NR_4^+-based electrolytes. However, our overall purpose was not solubility optimization, and we focused on **DGL-N-CH$_3$** due to ease of synthesis and the assumption that the other derivatives have

Research Article
doi.org/10.1002/batt.202400597
Chemistry Europe
European Chemical Societies Publishing

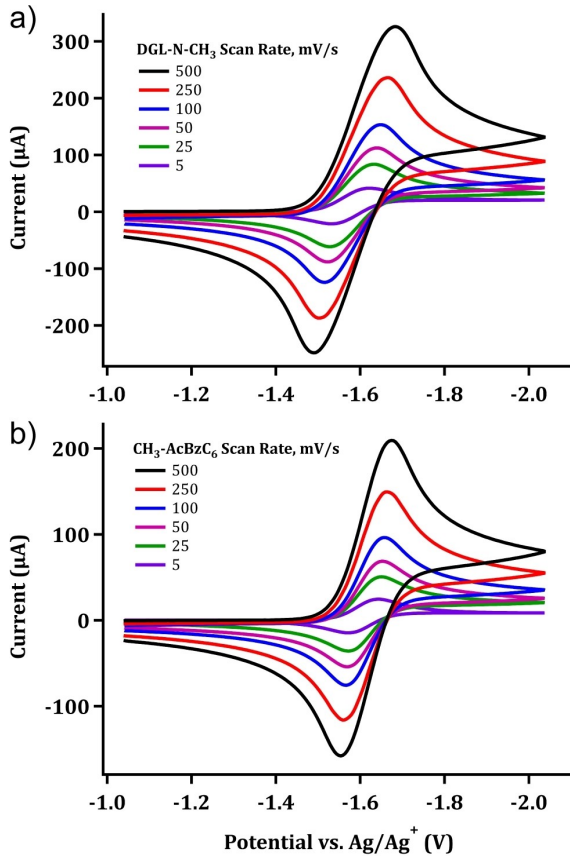

Figure 1. CV scan rate analysis of a) 10 mM **DGL-N-CH$_3$** (dimer) compared with b) 10 mM **CH$_3$-AcBzC$_6$** (monomer) in 0.5 M NBu_4PF_6 in CH_3CN.

similar electrochemical behavior. For example, **DGL-N-EG** had identical $E_{1/2}$ and diffusion coefficient of 2.3×10^{-5} cm^2/s (see the SI).

2.3. EPR Characterization

Electron paramagnetic resonance (EPR) spectroscopy is very helpful to characterize the kinetic stability and calendar lifetimes of charged redoxmers with unpaired electrons. We charged the dimer **DGL-N-CH$_3$** and monomer **CH$_3$-AcBzC$_6$** in 0.5 M NBu_4PF_6 solutions with 20 mM overall BzNSN unit concentration at a constant rate of 0.5 and 1C, respectively, to 100% state of charge (SOC) and obtained the decay kinetics of the paramagnetic species using EPR spectroscopy (see Sections S3 and S4). We estimated the calendar lifetimes of the subsequent **DGL-N-CH$_3$** dianion and **CH$_3$-AcBzC$_6$** anion (Figure 2). In 0.5 M NBu_4PF_6, the dianion of **DGL-N-CH$_3$** was stable and the lifetime controlled by diffusion of oxygen through the Teflon seals in the EPR tubes. By exponential extrapolation of kinetics observed before this incursion, we estimated $t_{1/2}$ ~1975 ± 20 h (~82 days); for comparison, **CH$_3$-AcBzC$_6$** has a $t_{1/2}$ of ~2160 ± 20 h (~90 days) (Figure 2a). Both redoxmers have similar broad EPR signals at the tested concentrations (Figures 2b and c).

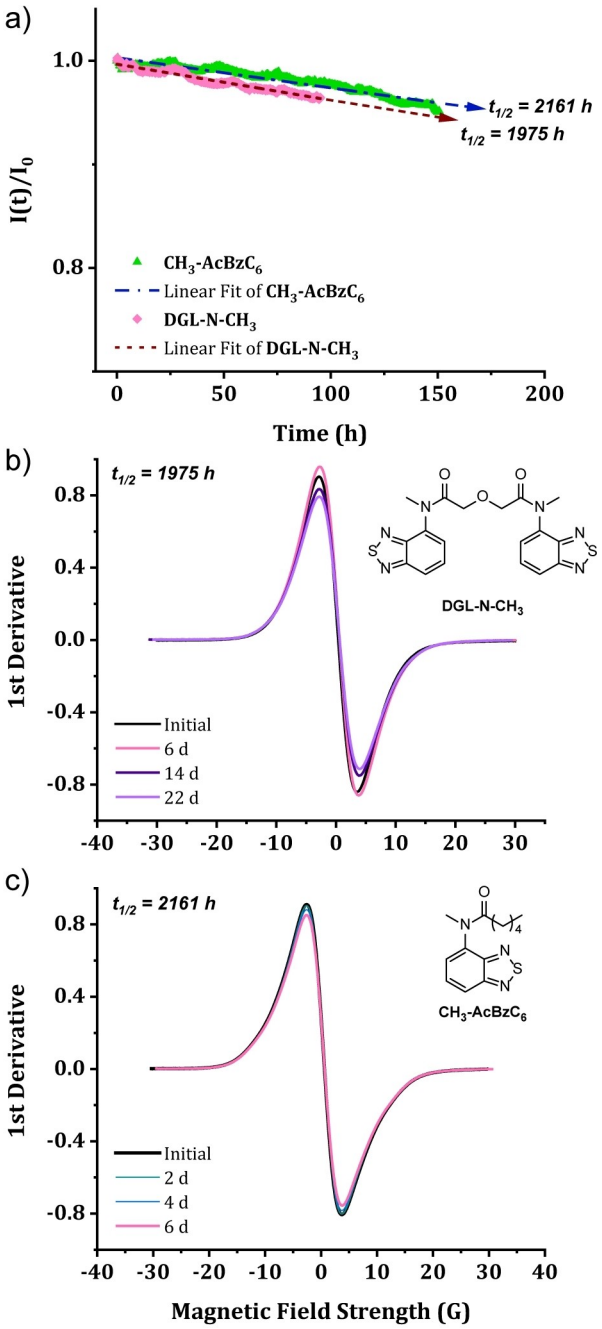

Figure 2. a) EPR-detected kinetics for 10 mM **DGL-N-CH$_3^{2\bullet-}$** (*pink diamonds*) and 20 mM **CH$_3$-AcBzC$_6^{\bullet-}$** (*green triangles*) in 0.5 M NBu_4PF_6 in CH_3CN after two-electron reduction of **DGL-N-CH$_3$** after charging at 0.5C and one-electron reduction of **CH$_3$-AcBzC$_6$** after charging at 1C. Small oscillations in the kinetics are due to temperature fluctuations. Linear fits are used to estimate the half-life times. Corresponding EPR spectra for b) 10 mM **DGL-N-CH$_3^{2\bullet-}$** and c) 20 mM **CH$_3$-AcBzC$_6^{\bullet-}$** in 0.5 M NBu_4PF_6 in CH_3CN after electrolysis.

The EPR spectra of **DGL-N-CH$_3^{2\bullet-}$** only show broad singlets. To resolve the spectrum, we diluted a 100% SOC 10 mM sample ten-fold in blank 0.5 M NBu_4PF_6 electrolyte. However, the EPR spectrum did not become resolved (Figure S3) and remained broad. Thus, the hyperfine splitting is not discernible for this species. For the case of the doubly charged species, this could

be due to dipole broadening or too small of hyperfine couplings.

2.4. Side Product Analysis of Charged DGL-N-$CH_3^{2\bullet-}$

As energized species, the charged states of redoxmers can form side products as they slowly decay. In the decomposition of $BzNSN^{\bullet-}$, the main product is *o*-phenylenediamine from protonation followed by sulfur extrusion.[16] We stored a 100% SOC sample of the dianion **DGL-N-$CH_3^{2\bullet-}$** in an argon-filled glovebox with periodic CV testing. The CV data (Figure 3) over one month showed a second, small reversible peak gradually emerged. We discharged a portion of this solution to determine the identity. The discharge was 71% of the original capacity (Figure S4), close to the 81% that would remain after one month from EPR estimation. Notably, the "100% SOC" solution, originally deep wine red in color, became light green upon discharge, which turned bright yellow after air exposure. The discharged electrolyte was analyzed by ^{1}H NMR spectroscopy and revealed a 5% pigment impurity in the 6.0–7.7 ppm range (Figure S5), which was identified as *N*-methyl-2,1,3-benzothiadiazol-4-amine (**$NHCH_3$-BzNSN**). This product may be generated via the N–C bond cleavage; indeed, the transformation of tertiary amides to aryl-amines using synthetic reducing agents or electrochemical means has been detailed.[17] This process likely occurs first by reduction of the carbonyl followed by cleavage at the nitrogen as observed for *N*-methyl-*N*-phenylacetamide, which converts 4% to these products after an 8-hr electrolysis. The **$NHCH_3$-BzNSN** product was also confirmed through direct synthesis (see Sections S1 and S5). The sulfur extrusion was not observed for either the monomer or dimer, indicating a different decay mechanism from the parent BzNSN molecule. As the main side product, **$NHCH_3$-BzNSN**, surprisingly still maintains a reversible redox behavior with a distinct potential at $E_{1/2} = -2.03$ V vs. Ag/Ag^+ (Figure S6), 0.15 V lower than that of **DGL-N-CH_3**, which matches with the new wave observed in the voltammograms of Figure 3.

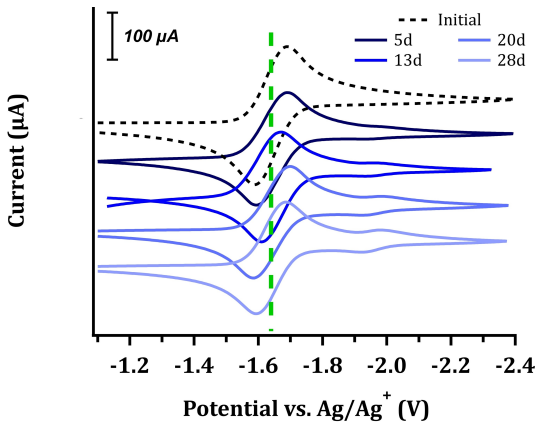

Figure 3. CV analysis over one month of a 100 SOC 10 mM **DGL-N-$CH_3^{2\bullet-}$** in 0.5 M NBu_4PF_6 in CH_3CN solution showing the evolution of a second peak. The green dashed line indicates the $E_{1/2}$ of the dimer.

2.5. UV-vis and Fluorescence

All DGL derivatives are strongly blue-green fluorescent. As expected, **DGL-N-CH_3** preserved the strong UV-vis absorbance at 335 nm (Figure 4a) and corresponding fluorescence emission at 495 nm (Figure 4b), similar to that of the monomer **CH_3-AcBzC$_6$**. We implemented the same crossover test using fluorescence for **DGL-N-Et** permeation through a microporous Daramic membrane as in our previous report (see Section S6 and Figure S7),[13] which revealed that the crossover permeability and diffusivity were similar to those of **CH_3-AcBzC$_6$** due to their similar hydrodynamic radius vs. the larger porosity of the Daramic membrane (Section S6 and Table S4). Interestingly, the pigment side product, **$NHCH_3$-BzNSN**, demonstrates very unique photophysics. The internal H-bond of **$NHCH_3$-BzNSN** formed between the amine hydrogen and the BzNSN nitrogen may cause planarization conformation (Figure 4b, inset), shielding of the ring protons in NMR, and leading to strong coloration (a 432 nm band with the molar extinction coefficient ~8.5×10^3 $M^{-1}cm^{-1}$). Also, **$NHCH_3$-BzNSN** preserved a bright orange fluorescence at 588 nm in electrolyte, contrasting with the blue-green fluorescence of the dimer with 93 nm shift as shown in Figure 4b. Such distinctive behavior makes **$NHCH_3$-BzNSN** an interesting FL indicator that could self-report side

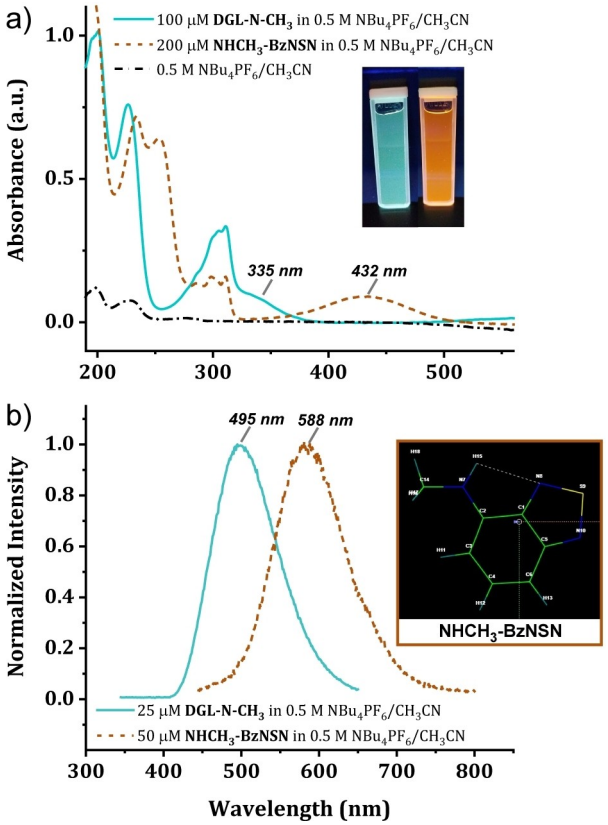

Figure 4. a) Absorbance and b) normalized fluorescence spectra for **DGL-N-CH_3** and **$NHCH_3$-BzNSN** in 0.5 M NBu_4PF_6 in CH_3CN (note: 1 mm path length cuvettes were used for absorbance data and 1 cm for fluorescence); panel b inset: structure of **$NHCH_3$-BzNSN** as predicted by DFT (b3lyp/6-31 + G**) showing the planar orientation of the molecule. *Color images:* the solutions from the absorbance experiment illuminated with 365 nm light.

product (itself) evolution and provides a unique opportunity to implement the "self-reporting" function towards associated capacity decay.

2.6. Self-Reporting State of Health (SOH)

In an RFB cell, the calendar life often provides the upper bound for cycling life as the latter also takes account for the side reactions on the electrodes or between different active species (such as crossover) during cycling.[18] Estimating the dynamic status parameters of an RFB cell, such as its SOH, is often a challenging task. SOH is an indication of the dynamic status of a battery, related to the initial condition of the battery. Typically, this initial condition is considered SOH = 100%. As time and usage of the battery increase (often referred as battery aging), the SOH will decrease. One critical measure for estimating SOH is the capacity decay. Diagnosing capacity decay, such as identifying redoxmer decomposition pathways, is critical for predicting and managing SOH of an RFB cell.[19]

The distinctive fluorescence of **NHCH$_3$-BzNSN** provides a possible way to self-report the redoxmer decomposition, which could be used to reflect SOH. To demonstrate, we adopted a symmetric H-cell setup with 2.5 mM **DGL-N-CH$_3$** (equivalent to 5 mM of BzNSN units) in 0.5 M NBu_4PF_6 in CH_3CN solution in each compartment. Reticulated vitreous carbon was used as the working and counter electrodes, and a quasi-reference Ag/$AgNO_3$ electrode was used to control the potential of the working electrode during the first charge (see Section S3 for more details). The cell was cycled using a two-electrode protocol, which avoids uncontrolled potentials in the counter chamber that lead to molecular degradation and artificial capacity decay. Specifically, constant current (cc) of 2.5 mA was applied for 100 cycles with the voltage cutoffs of ±0.85 V. The capacity was stable for 100 cycles at 0.31–0.32 mAh or 60% materials utilization (Figure 5a), which was also supported by the voltage vs. time profiles (Figure 5b), suggesting good stability of **DGL-N-CH$_3$**. The lower materials utilization is due to the higher applied current (equivalent to 5 mA/BzNSN, roughly 10C) used in H-cell studies.

Next, the H-cell cycling was continued to fully evaluate the formation of the pigment product over time. Under 2-electrode galvanostatic cycling at an initial 2.5 mA with ±0.85 V cutoffs, we removed aliquots of the electrolyte from both chambers after 100 and 400+ cycles (Figure 6). We then continued by running exhaustive cell cycling with voltage holds (cccv) for an additional 400 cycles, where the voltage holds are at ±0.85 V with ±5 μA limiting currents (Figure 6b). The current was adjusted after each aliquot to account for volume change. During the cccv portion of the cycling experiment, the overall cell resistance increases over 200 mV based on the voltage vs. time charge/discharge curves over the two weeks course of the experiment (Figures S8, S9). Before each aliquot, the cell was discharged to ensure that no reactive radical anions remained in the samples for analysis. Visually, a light yellow followed by green color appears on discharge with increasing cycle number (Figure 6c). The green color turns fully yellow when the samples

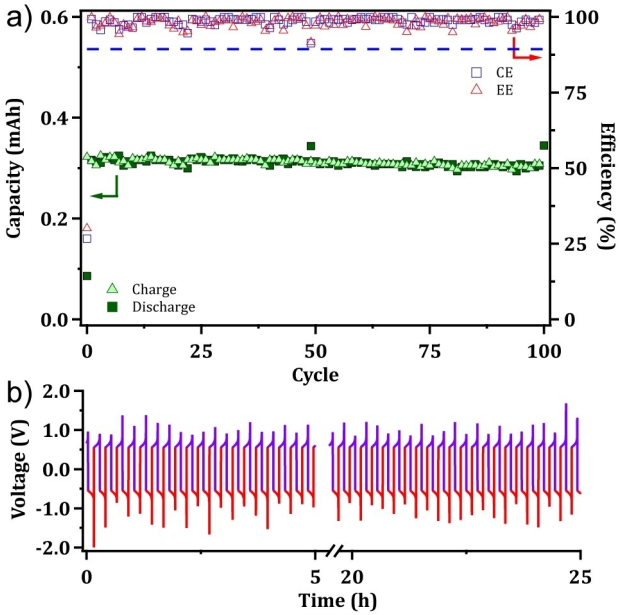

Figure 5. Two-electrode constant current H-cell cycling data for 2.5 mM **DGL-N-CH$_3$** (5 mM BzNSN units) in 0.5 M NBu_4PF_6 in CH_3CN at 2.5 mA: a) Capacity/efficiency profiles and b) corresponding voltage-time charge discharge curves. The blue-dashed line indicates the theoretical capacity.

are exposed to air. These discharged solutions were examined using CV and fluorescence spectroscopy (see Section S7). The cyclic voltammograms (Figure 6d) begin to show the dimer formation faintly at 100 cycles, but the formation is clearer by 400 cycles. The fluorescence analysis shows comparable results. For these experiments, the samples were diluted to 75 μM in CH_3CN with the assumption that the original solutions maintained 2.5 mM concentration and excited at 335 nm for **DGL-N-CH$_3$** and 443 nm for **NHCH$_3$-BzNSN**. For the 443 nm excitation, the emission corresponding to the amine product was observed at 100 cycles (Figure 6e). For the 335 nm excitation, the fluorescence intensity increased slightly over the course of the cycling experiment, possibly due to secondary "monomeric" species with the similar fluorescence but different quantum yield to the parent dimer (Figure S10).

Due to the low solubility of the model dimer compound, full flow cell studies were not performed. However, we note that the high sensitivity and selectivity of the fluorescence measurement is promising for detection of degradation products even earlier than cyclic voltammetry and UV-vis spectroscopy, where minor products may be masked by more dominant signals. We expect detection of the orange-emitting product even earlier than cycle 100. Additionally, small-scale synthetic tests on the synthesized **NHCH$_3$-BzNSN** show it undergoes complete conversion to N-acylated BzNSN derivatives (See Section S1 and Figure S16), indicating regenerative methods are also feasible and may be optically detected. These are precisely the properties we sought to illustrate "self-reporting" of the initial stages of material degradation. In this case, the "self-reporting" is achieved through fluorescence detection of a reaction product, but *any* property permitting

Research Article
doi.org/10.1002/batt.202400597
Chemistry Europe
European Chemical Societies Publishing

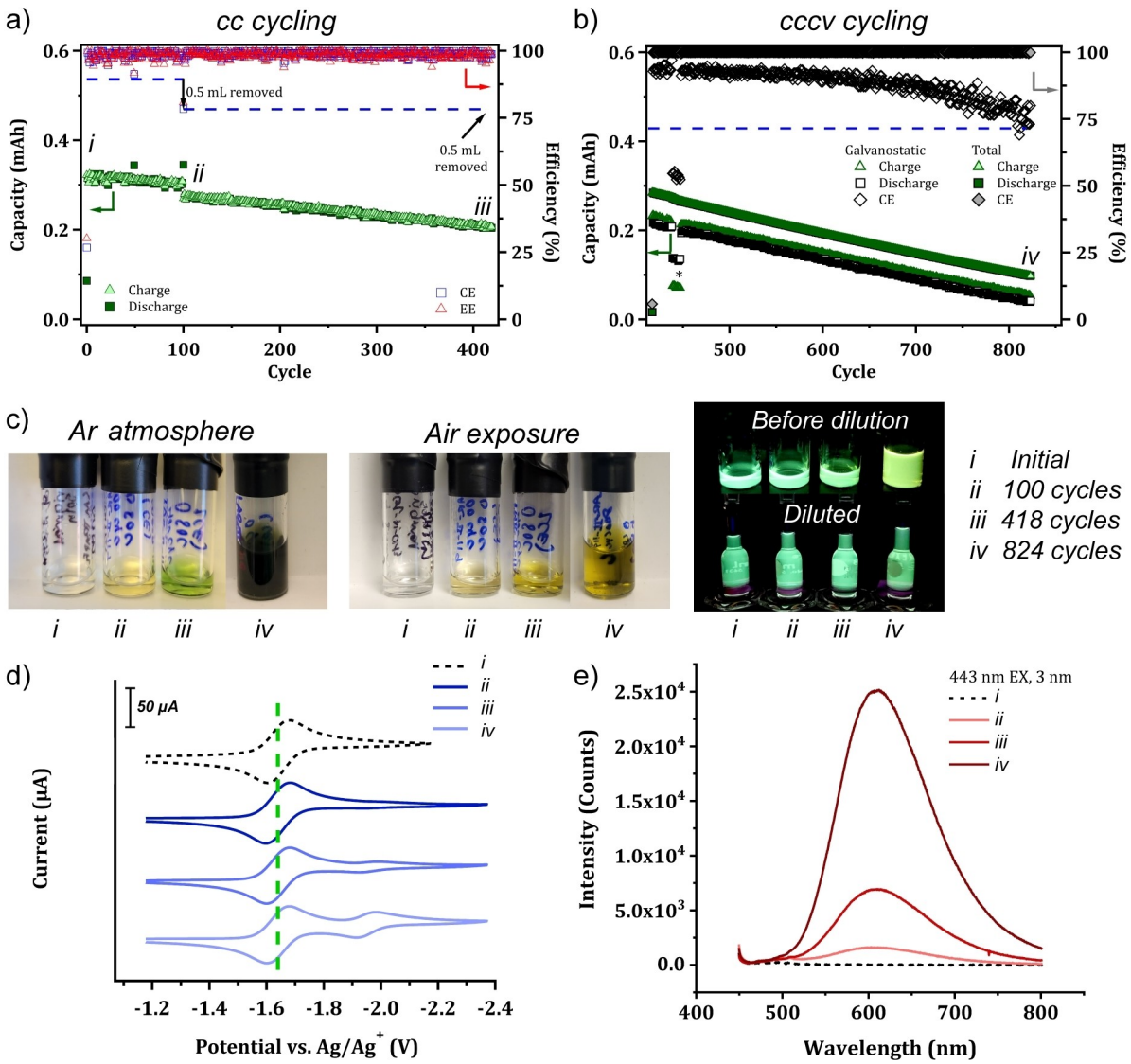

Figure 6. 2-Electrode H-cell cycling data for 2.5 mM **DGL-N-CH$_3$** in 0.5 M NBu_4PF_6 in CH_3CN at a) constant current for 400+ cycles with a 0.5 mL aliquot removed at 100 cycles and 400+ cycles and b) exhaustive constant current/constant voltage for an additional 400 cycles; c) color images of the aliquot samples under argon and air atmosphere (*left*); and excited with a 365 nm light before and after dilution (*right*); d) cyclic voltammograms of the aliquots at the original concentration; e). evolution of fluorescence signal at 443 nm (3 nm excitation and emission slit widths) corresponding to the **NHCH$_3$-BzNSN** product. *A stuck stir bar affected the mass transfer of the cell causing lower cc capacity. The Roman numerals *i-iv* indicate the time points of the data analysis.

advanced detection of degradation before it is observed through capacity fade would also be suitable.

3. Conclusions

In this study, a fluorescent BzNSN dimer with a diglycolamide linker, **DGL-N-CH$_3$**, was developed for constructing self-reporting functions for RFBs. While the dimer preserved most of the electrochemical and photophysical features from the monomer, such as low redox potential, decent stability, and strong fluorescence, a unique behavior was observed during EPR and H-cell cycling experiments. A minor side product, **NHCH$_3$-BzNSN**, was identified during EPR calendar life experiments, with ~1% formation after 1 month of storage. This product showed distinct electrochemical and fluorescence signatures and was also evident during cycling. By monitoring the evolution of the unique orange fluorescence from **NHCH$_3$-BzNSN**, we successfully detected the emerging of traces of this product at very early stage before the capacity decay became obvious or the product was evident by CV. Additionally, **NHCH$_3$-BzNSN** can be synthetically regenerated to an *N*-acyl BzNSN derivative. Such an approach, while in initial development, shows great promise for early diagnostics, and remediation, of parasitic reactions of RFB systems before their electrochemical signatures become apparent, representing one promising approach for monitoring the dynamic status of RFB systems and their early diagnosis of SOH.

Acknowledgements

The research was financially supported by the Joint Center for Energy Storage Research (JCESR), an Energy Innovation Hub funded by the U.S. Department of Energy, Office of Science, Basic Energy Sciences. The submitted manuscript has been created by UChicago Argonne, LLC, Operator of Argonne National Laboratory ("Argonne"). Argonne, a U.S. Department of Energy Office of Science laboratory, is operated under Contract No. DE-AC02-06CH11357. The U.S. Government retains for itself, and others acting on its behalf, a paid-up nonexclusive, irrevocable worldwide license in said article to reproduce, prepare derivative works, distribute copies to the public, and perform publicly and display publicly, by or on behalf of the Government. se of the Center for Nanoscale Materials, an Office of Science user facility, was supported by the U.S. Department of Energy, Office of Science, Office of Basic Energy Sciences, under Contract No. DE-AC02-06CH11357.

Conflict of Interests

The authors declare no conflict of interest.

Data Availability Statement

The data that support the findings of this study are available from the corresponding author upon reasonable request.

Keywords: Nonaqueous flow batteries · Redoxmers · Long-duration energy storage · Spectroscopy · State of health

[1] M. Arbabzadeh, R. Sioshansi, J. X. Johnson, G. A. Keoleian, *Nat. Commun.* **2019**, *10*, 3413.
[2] E. Sánchez-Díez, E. Ventosa, M. Guarnieri, A. Trovò, C. Flox, R. Marcilla, F. Soavi, P. Mazur, E. Aranzabe, R. Ferret, *J. Power Sources* **2021**, *481*, 228804.
[3] a) C. Jia, Q. Liu, C. J. Sun, F. Yang, Y. Ren, S. M. Heald, Y. Liu, Z. F. Li, W. Lu, J. Xie, *ACS Appl. Mater. Interfaces* **2014**, *6*, 17920–17925; b) N. Bevilacqua, L. Eifert, R. Banerjee, K. Köble, T. Faragó, M. Zuber, A. Bazylak, R. Zeis, *J. Power Sources* **2019**, *439*, 227071.
[4] K. Ngamsai, A. Arpornwichanop, *J. Power Sources* **2015**, *298*, 150–157.
[5] a) M. Skyllas-Kazacos, M. Kazacos, *J. Power Sources* **2011**, *196*, 8822–8827; b) R. P. Brooker, C. J. Bell, L. J. Bonville, H. R. Kunz, J. M. Fenton, *J. Electrochem. Soc.* **2015**, *162*, A608–A613; c) C. Petchsingh, N. Quill, J. T. Joyce, D. N. Eidhin, D. Oboroceanu, C. Lenihan, X. Gao, R. P. Lynch, D. N. Buckley, *J. Electrochem. Soc.* **2015**, *163*, A5068–A5083; d) W. Zhang, L. Liu, L. Liu, *RSC Adv.* **2015**, *5*, 100235–100243; e) L. Tong, Q. Chen, A. A. Wong, R. Gomez-Bombarelli, A. Aspuru-Guzik, R. G. Gordon, M. J. Aziz, *Phys. Chem. Chem. Phys.* **2017**, *19*, 31684–31691; f) D. G. Kwabi, A. A. Wong, M. J. Aziz, *J. Electrochem. Soc.* **2018**, *165*, A1770–A1776.
[6] a) V. I. Vlasov, M. A. Pugach, D. S. Kopylova, A. V. Novikov, N. A. Gvozdik, A. A. Mkrtchyan, A. I. Davletkhanov, Y. G. Gladush, F. M. Ibanez, D. A. Gorin, K. J. Stevenson, *J. Power Sources* **2023**, *584*, 233600; b) K. H. Shin, C. S. Jin, J. Y. So, S. K. Park, D. H. Kim, S. H. Yeon, *J. Storage Mater.* **2020**, *27*, 101066.
[7] E. W. Zhao, T. Liu, E. Jonsson, J. Lee, I. Temprano, R. B. Jethwa, A. Wang, H. Smith, J. Carretero-Gonzalez, Q. Song, C. P. Grey, *Nature* **2020**, *579*, 224–228.
[8] E. W. Zhao, E. Jonsson, R. B. Jethwa, D. Hey, D. Lyu, A. Brookfield, P. A. A. Klusener, D. Collison, C. P. Grey, *J. Am. Chem. Soc.* **2021**, *143*, 1885–1895.
[9] O. Nolte, R. Geitner, M. D. Hager, U. S. Schubert, *Adv. Energy Mater.* **2021**, *11*, 2100931.
[10] W. Duan, R. S. Vemuri, J. D. Milshtein, S. Laramie, R. D. Dmello, J. Huang, L. Zhang, D. Hu, M. Vijayakumar, W. Wang, J. Liu, R. M. Darling, L. Thompson, K. Smith, J. S. Moore, F. R. Brushett, X. Wei, *J. Mater. Chem. A* **2016**, *4*, 5448–5456.
[11] T. C. Gokoglan, S. K. Pahari, A. Hamel, R. Howland, P. J. Cappillino, E. Agar, *J. Electrochem. Soc.* **2019**, *166*, A1745–A1751.
[12] L. A. Robertson, M. Afsar Uddin, I. A. Shkrob, J. S. Moore, L. Zhang, *ChemSusChem* **2023**, *16*, e202300043.
[13] L. A. Robertson, I. A. Shkrob, G. Agarwal, Y. Zhao, Z. Yu, R. S. Assary, L. Cheng, J. S. Moore, L. Zhang, *ACS Energy Lett.* **2020**, *5*, 3062–3068.
[14] C. M. Davis, C. E. Boronski, T. Yang, T. Liu, Z. Liang, *Batteries* **2023**, *9*, 504.
[15] a) M. J. Baran, M. N. Braten, E. C. Montoto, Z. T. Gossage, L. Ma, E. Chénard, J. S. Moore, J. Rodríguez-López, B. A. Helms, *Chem. Mater.* **2018**, *30*, 3861–3866; b) K. H. Hendriks, S. G. Robinson, M. N. Braten, C. S. Sevov, B. A. Helms, M. S. Sigman, S. D. Minteer, M. S. Sanford, *ACS Cent. Sci.* **2018**, *4*, 189–196.
[16] a) J. Zhang, J. Huang, L. A. Robertson, R. S. Assary, I. A. Shkrob, L. Zhang, *J. Phys. Chem. C* **2018**, *122*, 8116–8127; b) B. A. D. Neto, A. A. M. Lapis, E. N. da Silva Júnior, J. Dupont, *Eur. J. Org. Chem.* **2013**, *2013*, 228–.
[17] a) K. Rix, *Imperial College London (London)*, **2013**; b) W. Yao, L. He, D. Han, A. Zhong, *J. Org. Chem.* **2019**, *84*, 14627–14635.
[18] W. Duan, J. Huang, J. A. Kowalski, I. A. Shkrob, M. Vijayakumar, E. Walter, B. Pan, Z. Yang, J. D. Milshtein, B. Li, C. Liao, Z. Zhang, W. Wang, J. Liu, J. S. Moore, F. R. Brushett, L. Zhang, X. Wei, *ACS Energy Lett.* **2017**, *2*, 1156–1161.
[19] L. Ungurean, G. Cârstoiu, M. V. Micea, V. Groza, *Int. J. Energy Res.* **2017**, *41*, 151–181.

Manuscript received: September 6, 2024
Revised manuscript received: October 24, 2024
Accepted manuscript online: November 1, 2024
Version of record online: November 21, 2024

